Chemical and Process Engineering: New Frontiers, 2024, 45(4), e76
DOI: 10.24425/cpe.2024.149471

Enhancing carbon dioxide adsorption in a hybrid fixed bed via structuring and thermal management: a numerical study

Enrico A. Cutillo[1], Krzysztof Neupauer[1], Gaetano Continillo[1], Katarzyna Bizon[2]*

[1] Università degli Studi del Sannio, Department of Engineering, Piazza Roma 21, 82100 Benevento, Italy
[2] Cracow University of Technology, Faculty of Chemical Engineering and Technology, ul. Warszawska 24, 31-155 Kraków, Poland

*** Corresponding author, e-mail:** katarzyna.bizon@pk.edu.pl

Presented at
4rd Seminar on Practical Aspects of Chemical Engineering PAIC 2024, 16–17 May 2024, Zaniemyśl, Poland. Guest Editors: Andżelika Krupińska and Sylwia Włodarczak.

Article info:
Received: 19 July 2024
Revised: 23 September 2024
Accepted: 09 October 2024

Abstract
Systems based on physical sorption are an attractive solution for CO_2 capture from flue gases, biogas upgrading or gas storage. Besides the sorbent choice, one of the most important factors related to the design of such systems is proper heat management. Commonly used sorbents typically have low thermal conductivity. Nevertheless, catalyst particles characterized by high conductivity are inherently present in adsorptive (hybrid) reactors. Thus, appropriate structuring of hybrid beds can be used for controlling temperature profiles and improving the bed performance. In this study, the behaviour of a nonadiabatic adsorptive reactor described by a two-dimensional model was analysed for the adsorption step. The effect on the CO_2 adsorption performance of different spatial distributions of functionalities in the bed was investigated. The optimality problem for nonuniform radial distribution of sorbent and catalyst in the bed was solved, indicating that such a configuration is a potentially important direction for structuring hybrid beds. Results demonstrate that the optimal configuration of radially distributed functionalities significantly increases the amount of CO_2 absorbed under identical boundary and initial conditions for the bed. It appears that precise control of the heat generated and removed from the bed is achievable. Such control could be advantageous for the regeneration phase.

Keywords
CO_2 sequestration, hybrid fixed bed, structured bed, thermal management, adsorptive reactor optimization

1. INTRODUCTION

The need for deceleration of ongoing global warming and the urgency for energy transition demand the development of new technologies as well as the advancement of existing ones. Among the techniques that undoubtedly require rapid development are various methods for separating carbon dioxide and other greenhouse gases, including volatile organic compounds (VOCs), from flue gases and ambient air. Another important and urgent problem to be addressed is the issue of treating fuels of biological origin and in particular, the upgrading of biogas to biomethane. Ultimately, in light of the pursuit of widespread use of hydrogen and methane as fuel, it is also necessary to develop safe and viable (in terms of energy density) methods of both stationary and on-board storage of these fuels. An attractive solution suitable for CO_2 capture (Ben-Mansour et al., 2020), biogas upgrading (Abd et al., 2024) or gas storage (Grande et al., 2023) are undoubtedly adsorption-based systems. Another example of the use of adsorption systems that is in line with eco-friendly and sustainable development concepts are adsorption-based cooling systems (Chauhan et al., 2022; Szyc and Nowak, 2014).

It is worth noting that physical adsorption together with chemisorption, membrane and cryogenic separation (Kammerer et al., 2023) provide the foundation for carbon capture and storage (CCS) and carbon capture and utilization (CCU) methods (Leonzio and Shah, 2024; McLaughlin et al., 2023). Three fundamental storage methods for CO_2 falling under the CCS concept are generally available, namely oceanic, geological and mineral storage (Lin et al., 2024). In recent years the latter, also known as mineral carbonation, gained particular attention. It involves the binding of CO_2 with alkali and alkaline earth metal oxides, such as magnesium oxide and calcium oxide. Unlike geological storage, the process of carbonation takes place on the ground and yields a product that is stable over a long period. While the method itself is very attractive, primarily due to its safety, its application on a larger scale requires further intensive work. This is primarily due to the low reaction rate of mineral carbonation (Lin et al., 2024). On the other hand, CCU techniques involve reusing CO_2 and converting it into valuable chemicals, including fuels, polymers or feedstock chemicals such as formic acid (McLaughlin et al., 2023). Among the various options, the conversion of CO_2 to methane provides both a way to prevent its emission to atmosphere and to chemically store surplus energy generated from renewable sources (Miguel et al., 2017). There are three basic modes of implementation of CO_2 methanation, that is: direct methanation, sorption-enhanced methanation with in-situ water removal, and the recently proposed cyclic capture of CO_2 and its conversion in the same unit. In particular, the latter approach still requires research centred on the appropriate combination of adsorptive and catalytic functions in the apparatus.

Although studies involving the use of adsorbents for gas separation and storage have been the subject of extensive research for many decades, there are still many challenges in this field. They are strongly aligned with the goals and requirements imposed on the technologies under development. In fact, the crucial features that are expected to accompany the technologies of the future are essentially process integration and intensification, miniaturization, energy efficiency and zero waste. In this regard, one aspect that needs to be further researched extensively is increasing the capacity of adsorption systems, which can be realized both through the preparation of novel sorbents and, at the apparatus level, by choosing appropriate conditions for the execution of the process. Given that adsorption is an exothermic process and desorption is an endothermic process, the critical element that determines the efficiency of the sorption process is the heat removal and supply at the adsorption and desorption stages, respectively (Ben-Mansour et al., 2020; Kwan and Yao, 2022). Gas uptake and sorption efficiency are heavily influenced by heat transport in the bed of a solid sorbent, which is significantly hindered because of the low values of thermal conductivity of typical adsorbents (Saha et al., 2019).

To address the aforementioned problem, various heat management concepts aimed at improving heat transfer in granular beds were proposed and studied (Ben-Mansour et al., 2020; Demir et al., 2010; Grande et al., 2023), ranging from external (Fig. 1a), annular (Fig. 1b) and internal (Fig. 1c) water-cooling systems, or various combinations of them (Fig. 1d), longitudinal (Fig. 1e) or transversal fins (Fig. 1f), 3D printed metal lattices (Fig. 1g) or use of metal additives in the form of tiny chips. Also, the geometry of the apparatus itself affects the uptake of adsorbate captured from the gas being purified. In addition to obvious features such as the ratio of the apparatus diameter to its length, which, as shown in the literature (Lian et al., 2019), significantly affects the removal of heat from the bed generated in the exothermic adsorption process, an interesting solution is the structuring of the walls of the apparatus (Fig. 1h). In fact, it is known that in fixed beds randomly filled with particles, the bed void fraction near the walls is higher than in the axis of the apparatus, which negatively affects the heat transfer process (van Antwerpen et al., 2010). Hence, the design of a properly structured wall makes it possible to equalize the distribution of porosity in the radial direction of the apparatus, which, as a result, improves the heat removal rate from the bed (Eppinger et al., 2021).

Referring to bed additives (e.g. aforementioned metal chips) characterized by high conductivity and acting as a heat sink, in addition to inert materials, it is also worth mentioning hybrid beds consisting of an adsorbent and a catalyst. The latter can be used, for example, to conduct cyclic processes of CO_2 adsorption and its subsequent methanation in the Sabatier reaction (Martins et al., 2022). Another example of the use of adsorptive reactors for the capture of one compound in the first step, followed by a second step in which the conversion of the captured compound takes place, is the process of VOC capture, followed by their catalytic oxidation as described by Jarczewski et al. (2022). Appropriate tailoring of hybrid fixed beds in adsorptive (hybrid) reactors, e.g. in terms of the ratio of adsorbent to catalyst or in terms of the spatial arrangement of various functionalities, can also help to control the temperature profiles in the apparatus and thus improve process performance.

Given the above, the aim of this study was to assess the performance of a nonadiabatic adsorptive reactor operating at the CO_2 adsorption step and characterized by different spatial distributions of functionalities, which are zeolite 13X adsorbent and nickel catalyst. The evaluation of the spatial arrangement of particles characterized by different values of thermal conductivity and heat capacity was conducted by means of dynamic simulations using a two-dimensional model. Moreover, the optimality problem for radially nonuniform adsorbent distribution in the bed was solved. To find the global optimum that meets the constraints, a numerical method was implemented by discretizing the feasible space of the control variables using a uniform grid. Strictly speaking, this allowed to find a sub-optimal solution in the set of values of the discretized variables.

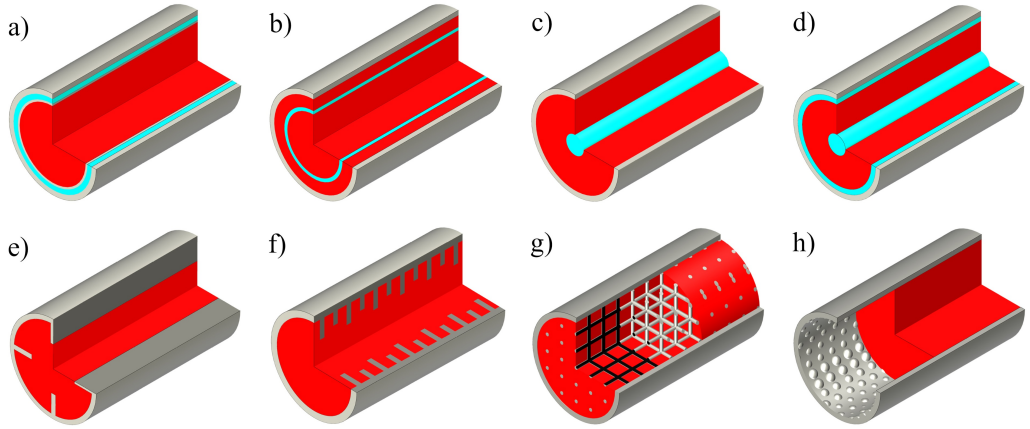

Figure 1. Schematic of different configurations of fixed-bed adsorbent column: (a) bed with cooled wall, (b) bed with annular cooling, (c) bed with inner cooling, (d) bed with cooled wall and inner cooling, (e) bed with longitudinal fins, (f) bed with annular fins, (g) bed with internal lattice, (h) bed with structured wall.

2. MATHEMATICAL MODEL AND NUMERICAL PROCEDURE

While in a previous study (Gunia et al., 2023), the effect of the macrostructure of an adiabatic hybrid fixed bed on carbon dioxide adsorption efficiency was evaluated using one-dimensional mathematical model, in this study the analysis was further extended to the nonadiabatic two-dimensional case to account for both longitudinal and radial distributions of concentration and temperature.

The impact of different spatial arrangements of sorbent and catalyst in the hybrid bed on its performance at the CO_2 adsorption step was investigated. The arrangements analysed are as follows:

- a bed made of a uniform physical mixture of adsorbent and catalyst particles (Fig. 2a),
- a bed composed of alternating layers of adsorbent and catalyst particles (Fig. 2b),
- a bed with radially nonuniform distribution of adsorbent and catalyst particles (Fig. 2c).

2.1. Model assumptions and governing equations

The following simplifying assumptions were adopted to formulate the mathematical model of the hybrid bed:

- a cylindrical fixed-bed hybrid apparatus is described using a two-dimensional axisymmetric model, thus both axial and radial variations of concentration and temperature are considered,
- the system is assumed to be adiabatic, with bed-to-wall heat transport being described by the α_w-model (Stegehake et al., 2018; Yagi and Kunii, 1960),
- there is a local thermal equilibrium of the gas phase and the solid phase, i.e. adsorbent and catalyst particles, consequently, from the thermal point of view, the model has a pseudo-homogeneous character,
- the gas mixture being separated via adsorption contains only CO_2 and N_2, moreover the inlet concentration of the component that is adsorbed (CO_2), is low enough to assume a constant gas velocity during its flow through the bed,
- the gas obeys the ideal gas law, and the pressure drop is low enough to be neglected,
- the gas flow is accompanied by both axial and radial dispersion of the mass,
- the Toth isotherm is employed to describe the adsorption equilibrium, and the rate of mass transfer is given by the linear driving force (LDF) model,
- in the energy balance, in addition to the convective component, axial and radial heat conduction resulting from the thermal conductivity of solid particles and gas, as well as from gas motion, is also considered,
- values of physical, thermal and transport properties are independent of temperature and calculated with respect to averaged concentrations and temperatures.

Under the above assumptions, the mass and energy equations describing the analysed system are as follows:

$$\frac{\partial C_{CO_2}}{\partial t} = \frac{1}{\Gamma_{mass}}\left[\varepsilon_b D_{ax}\frac{\partial^2 C_{CO_2}}{\partial x^2} + \frac{\varepsilon_b D_{rad}}{r}\frac{\partial}{\partial r}\left(r\frac{\partial C_{CO_2}}{\partial r}\right) - u\frac{\partial C_{CO_2}}{\partial x} - \rho_{b,ads} f_{ads}\frac{\partial q_{CO_2}}{\partial t}\right] \tag{1}$$

$$\frac{\partial T}{\partial t} = \frac{1}{\Gamma_{heat}}\left[K_{ax}\frac{\partial^2 T}{\partial x^2} + \frac{K_{rad}}{r}\frac{\partial}{\partial r}\left(r\frac{\partial T}{\partial r}\right) - u\rho_g c_g\frac{\partial T}{\partial x} + \rho_{b,ads} f_{ads}\left(-\Delta H_{ads}\right)\frac{\partial q_{CO_2}}{\partial t}\right] \tag{2}$$

where:

$$\Gamma_{mass} = \varepsilon_{t,ads} f_{ads} + \varepsilon_{t,cat} f_{cat} \tag{3}$$

$$\Gamma_{heat} = \left(\varepsilon_{t,ads} f_{ads} + \varepsilon_{t,cat} f_{cat}\right)\rho_g c_g + \rho_{b,ads} f_{ads}\left(c_{s,ads} + c_{g,ads}\right) + \rho_{b,cat} f_{cat} c_{s,cat} \tag{4}$$

where f_{ads} denotes the volume fraction of adsorbent particles, whereas $f_{cat} = 1 - f_{ads}$ is the volume fraction of catalyst particles in the hybrid bed.

The adsorption rate $\partial q_{CO_2}/\partial t$ was described by the linear driving force (LDF) model (Glueckauf and Coates, 1947), namely:

$$\frac{\partial q_{CO_2}}{\partial t} = k\left(q^*_{CO_2} - q_{CO_2}\right) \tag{5}$$

where:

$$k = \frac{15 D_e}{r_p^2} \quad \text{and} \quad D_e = \frac{\varepsilon_p}{\tau_p}\frac{D_K D_m}{D_K + D_m} \tag{6}$$

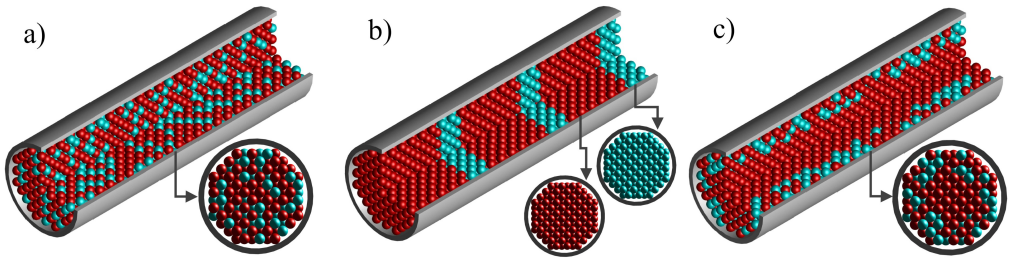

Figure 2. Different configurations of a hybrid bed formed of adsorbent and catalyst particles: (a) uniform mixture of particles, (b) bed made of alternating layers of adsorbent and catalyst, and (c) radially nonuniform distribution of both types of particles. Blue spheres indicate catalyst and red spheres indicate adsorbent.

with the molecular diffusion coefficient, D_m, calculated from the formula proposed by Chapman and Enskog (Poling et al., 2001), and Knudsen diffusion coefficient, D_K, calculated using the formula based on the kinetic theory of gases (Do, 1998).

The equilibrium concentration in Eq. (5) was described with Toth isotherm for zeolite 13X (Wang and LeVan, 2009) given by the following equation:

$$q^*_{CO_2} = \frac{a p_{CO_2}}{\left[1 + \left(b p_{CO_2}\right)^{\tau}\right]^{1/\tau}} \tag{7}$$

where:

$$a = a_0 \exp\left(\frac{E}{T}\right) \quad b = b_0 \exp\left(\frac{E}{T}\right) \quad \tau = \tau_0 + \frac{c}{T} \tag{8}$$

The coefficient of axial mass dispersion, D_{ax}, which appears in the mass balance given by Eq. (1) was calculated based on the following correlation (Wakao and Funazkri, 1978):

$$D_{ax} = \frac{D_m}{\varepsilon_b}\left(20 + 0.5 \mathrm{Sc} \mathrm{Re}_p\right) \tag{9}$$

while the radial dispersion coefficient, D_{rad}, was calculated using the following expression (Tsotsas and Schlünder, 1990):

$$D_{rad} = D_m\left(1 - \sqrt{1 - \varepsilon_b}\right) + \frac{u d_p}{8} \tag{10}$$

To simplify the calculations, constant values of density, ρ_g, and viscosity, μ_g, (determined based on the average composition and temperature of the gas mixture) were used to determine Schmidt and Reynolds numbers in Eq. (9). An analogous approach was made for the specific heat capacity of the gas phase, c_g, and adsorbed phase, $c_{g,ads}$, and for the enthalpy of adsorption, ΔH_{ads}. The latter was calculated, for the averaged saturation of the solid, from the Clausius–Clapeyron equation, which is (Do, 1998):

$$-\Delta H_{ads} = \frac{RT^2}{p_{CO_2}}\left(\frac{\partial p_{CO_2}}{\partial T}\right)_{q^*_{CO_2}}$$
$$\text{where} \quad p_{CO_2} = \frac{q^*_{CO_2}}{\left[a^{\tau} - \left(q^*_{CO_2}\right)^{\tau}\right]^{1/\tau}} \tag{11}$$

The values of axial, K_{ax}, and radial, K_{rad}, effective thermal conductivities were determined from the following correlations (Kunii and Smith, 1960; Yagi et al., 1960):

$$K_{ax} = K^0_{ax} + \lambda_g a_{ax} \mathrm{Pr}\, \mathrm{Re}_p \tag{12}$$
$$K_{rad} = K^0_{rad} + \lambda_g a_{rad} \mathrm{Pr}\, \mathrm{Re}_p \tag{13}$$

In the above Equations (12) and (13), the first term denotes the so-called stagnant thermal conductivity, while the second term accounts for the effect of gas flow motion on heat transport. The parameters a_{ax} and a_{rad} are empirical parameters; in the present study, following the literature results (Díaz-Heras et al., 2020), values equal to $a_{ax} = 0.5$ and $a_{rad} = 0.1$ were adopted. The stagnant thermal conductivity was calculated assuming that the medium is isotropic, therefore the radial and axial stagnant thermal conductivities were considered equal (Díaz-Heras et al., 2020) and were calculated as follows (Kunii and Smith, 1960):

$$K^0_{ax} = K^0_{rad} = \varepsilon_b + \frac{\beta(1 - \varepsilon_b)}{\psi_t + \gamma/\kappa}$$
$$\text{where} \quad \beta = 0.9 \quad \text{and} \quad \kappa = \frac{\lambda_s}{\lambda_g} \tag{14}$$

whereas ψ_t depends on the bed porosity and the number of contact points between particles; for details on determining this quantity, see (Díaz-Heras et al., 2020; Gunia et al., 2023; Kunii and Smith, 1960).

The solution of the system of partial differential equations (PDEs) given by Eqs. (1) and (2), together with Eq. (5), which was also used to determine the amount of CO_2 adsorbed, requires the definition of appropriate boundary conditions and initial conditions. Therefore, the boundary conditions (for the adsorption step) were defined as:

$$-D_{ax}\frac{\partial C_{CO_2}}{\partial x} = \frac{u}{\varepsilon_b}\left(C_{f,CO_2} - C_{CO_2}\right)$$
$$\text{at} \quad x = 0 \quad \text{and} \quad \forall r \in [0, R_r] \tag{15}$$
$$\frac{\partial C_{CO_2}}{\partial x} = 0 \quad \text{at} \quad x = L \quad \text{and} \quad \forall r \in [0, R_r] \tag{16}$$
$$\frac{\partial C_{CO_2}}{\partial r} = 0 \quad \text{at} \quad r = 0 \quad \text{and} \quad \forall x \in [0, L] \tag{17}$$
$$\frac{\partial C_{CO_2}}{\partial r} = 0 \quad \text{at} \quad r = R_r \quad \text{and} \quad \forall x \in [0, L] \tag{18}$$
$$-K_{ax}\frac{\partial T}{\partial x} = u \rho_g c_g \left(T_f - T\right)$$
$$\text{at} \quad x = 0 \quad \text{and} \quad \forall r \in [0, R_r] \tag{19}$$
$$\frac{\partial T}{\partial x} = 0 \quad \text{at} \quad x = L \quad \text{and} \quad \forall r \in [0, R_r] \tag{20}$$
$$-K_{rad}\frac{\partial T}{\partial r} = h_w\left(T - T_w\right)$$
$$\text{at} \quad r = 0 \quad \text{and} \quad \forall x \in [0, L] \tag{21}$$
$$\frac{\partial T}{\partial r} = 0 \quad \text{at} \quad r = R_r \quad \text{and} \quad \forall x \in [0, L] \tag{22}$$

Assuming that, initially, interparticle voids and intraparticle pores are filled with an inert gas, the initial conditions are:

$$C_{CO_2}(x, r, 0) = q_{CO_2}(x, r, 0) = 0$$
$$\text{and } T(x, r, 0) = T_0 \quad \forall x \in [0, L] \text{ and } \forall r \in [0, R_r] \tag{23}$$

The Robin-type boundary condition defined by Eq. (21) used to describe the energy exchange between the bed and the wall originates from the so-called α_w-model (Stegehake et al., 2018; Yagi and Kunii, 1960), which constitutes one approach for modelling cooled fixed-bed. The simplifying hypothesis behind the α_w-model implies that porosity, flow, and effective heat and mass dispersion are independent of radial position.

Although the α_w-model exhibits inherent limitations that cannot be overcome by more accurate estimation of transport parameters, such as the unphysical temperature gradient between the near-wall region and the reactor wall, it is commonly used in practical applications due to its relatively low computational burden (Stegehake et al., 2018) and the possibility of obtaining an analytical solution of the heat transfer equation under certain simplifying hypotheses (Dixon et al., 1978; Jorge et al., 2010). The selection of the α_w-model in this study was further justified by the fulfilment of two conditions: first, the inner diameter of the reactor significantly exceeds the diameter of the particles ($D_r/d_p > 15$) (Stegehake et al., 2019); second, the adsorption process is not highly exothermic.

The apparent wall heat transfer coefficient, h_w, found on the right side of Eq. (21) was calculated according to the following formula recommended by Dixon (2012):

$$\mathrm{Nu}_w = \mathrm{Nu}_{w0} + \frac{1}{(1/\mathrm{Nu}_w^*) + (1/\mathrm{Nu}_m)} \tag{24}$$

where:

$$\mathrm{Nu}_{w0} = \left(1.3 + \frac{5}{D_r/d_p}\right)\left(\frac{K_{\mathrm{rad}}^0}{\lambda_g}\right) \tag{25}$$

$$\mathrm{Nu}_w^* = 0.3\mathrm{Pr}^{0.33}\mathrm{Re}_p^{0.8} \tag{26}$$

$$\mathrm{Nu}_m = 0.054\,\mathrm{Pr}\,\mathrm{Re}_p \tag{27}$$

Substituting Eq. (25)–(27) into Eq. (24) and using the definition of Nusselt number yields the formula:

$$h_w = \frac{\lambda_g}{d_p}\left(\mathrm{Nu}_{w0} + \frac{1}{(1/\mathrm{Nu}_w^*) + (1/\mathrm{Nu}_m)}\right) \tag{28}$$

2.2. Numerical solution of the model and employed parameters

To solve numerically the equations of the model, which consist of two PDEs (Eqs. (1) and (2), an ordinary differential equation (ODE, Eq. (5)) to be solved at each position of the domain, with the associated boundary (Eqs. (15)–(22)) and initial conditions (Eq. (23)), the method of lines was applied. It consists in approximating the derivatives with respect to spatial variables at discrete grid nodes using finite differences. The resulting large system of ODEs is then solved using an appropriate solver. In the present study, the spatial domain, that is, half of the cross-section of a tubular reactor, was discretized using $N_{\mathrm{ax}} \cdot N_{\mathrm{rad}} = 251 \cdot 51 = 12801$ nodes, where N_{ax} refers to the number of nodes along the bed length and N_{rad} along its radius. The obtained system of ODEs was then solved using the *ode15s* solver of the MATLAB software. To improve the reliability and efficiency of stiff ODE solvers (such as *ode15s*), providing information about the Jacobian matrix is crucial. The open-source ADiGator package developed in MATLAB was therefore used to generate the Jacobian sparsity pattern of the obtained ODE system, which is useful to numerically calculate a sparse Jacobian, significantly reducing the computational time (Weinstein and Rao, 2017).

In the case of the bed made of alternating layers of adsorbent and catalyst (Fig. 2b), f_{ads} is solely a function of axial coordinate, x, and it was defined as in the previous work (Gunia et al., 2023) as a combination of double sigmoid functions:

$$f_{\mathrm{ads}}(x) = 1 - \sum_{i=1}^{M/2-1} \frac{1}{1+\exp\left[-A\left(x - x_{2i-1}\right)\right]} \cdot \frac{1}{1+\exp\left[A\left(x - x_{2i}\right)\right]} - \frac{1}{1+\exp\left[-A\left(x - x_{M-1}\right)\right]} \tag{29}$$

where M denotes the total number of layers of different material within the bed, x_i is the endpoint coordinate of the layer, whereas A is the sigmoid slope. In this study the value of A was set to 10000. This choice was guided by the objective of defining a function that closely resembles a step function while avoiding convergence errors.

The adsorbent distribution, $f_{\mathrm{ads}}(x)$, defines the fraction of the reactor volume dedicated to the presence of the adsorbent. Its complement to unity represents the distribution function of the catalyst (or inert) material, i.e. $f_{\mathrm{cat}}(x) = 1 - f_{\mathrm{ads}}(x)$. It is important to note that f_{ads} is not simply the ratio of adsorbent volume to total reactor volume, but rather the ratio of the reactor volume dedicated to adsorbent particles to the total reactor volume, $V_{\mathrm{tot}} = L\pi R_r^2$. The expression "dedicated volume" includes both solid particles and voids. When filled with adsorbent, this designated volume of the reactor includes both the actual sorbent material (solid fraction) and the interparticle voids (void fraction).

For the case of the bed with radially nonuniform distribution of both types of particles, only the cases that are assumed feasible under practical conditions were adopted. Namely, it was assumed that the bed consists of an inner cylindrical core with a diameter of $R_c < R_r$, in which $f_{\mathrm{ads},1}$ and, consequently, $f_{\mathrm{cat},1}$ are constant values, encircled by a cylindrical shell, in which the distributions of individual functionalities ($f_{\mathrm{ads},2}$, $f_{\mathrm{cat},2}$) are also constant, but with values different from those in the core. Such a distribution, which in this case is only a function of the radial coordinate, is described by the following function:

$$f_{\mathrm{ads}}(r) = \frac{f_{\mathrm{ads},1}}{1+\exp[A(r-R_c)]} + \frac{f_{\mathrm{ads},2}}{1+\exp[-A(r-R_c)]} \tag{30}$$

Figure 3a shows representative distributions of both materials in the bed corresponding to the optimal case described later in this study. It is important to underline that in the configuration where the distribution of functionalities varies radially, once the adsorbent-to-catalyst ratio is defined and $f_{\mathrm{ads},1}$ are defined, the other constant $f_{\mathrm{ads},2}$ is also determined indirectly as a function of the other two parameters. This relation is crucial for the optimization process because it reduces the number of feasible solutions, i.e. it represents a constraint of the optimization problem.

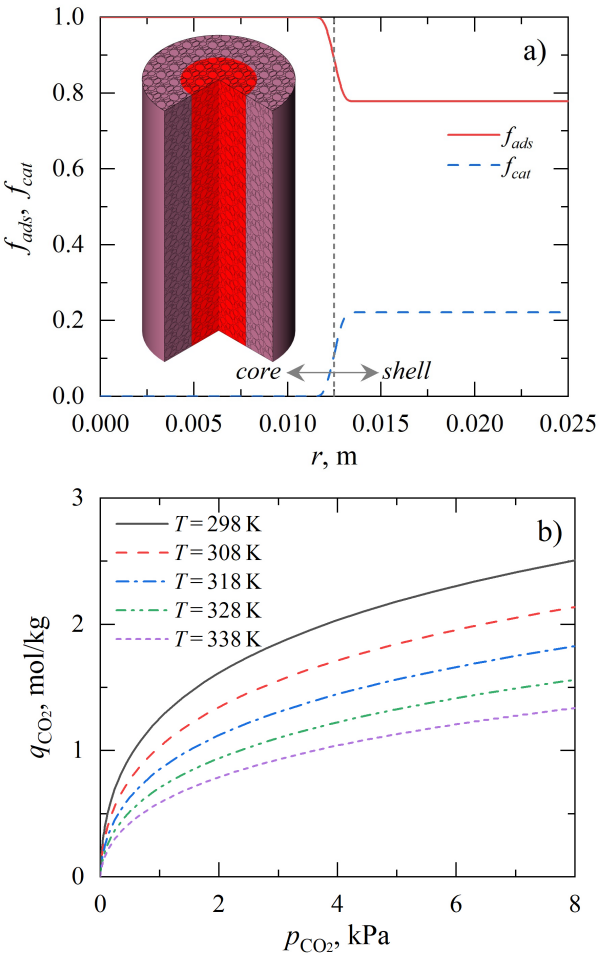

Figure 3. Radial distributions of adsorbent and catalyst volume ratio in configuration with the radially nonuniform sorbent distribution (a), and adsorption isotherms of CO_2 on zeolite 13X (b) determined for different temperatures based on parameters from Wang and LeVan (2009).

The main parameters of the mathematical model used in the numerical simulations are summarized in Table 1. In addition, Fig. 3b graphically shows the isotherms of CO_2 adsorption on zeolite 13X, which were calculated based on the parameters given in the work of Wang and LeVan (2009). The physical parameters of the second granular material, i.e. nickel catalyst, which has an inert character during the adsorption stage, were taken from Bremer et al. (2017).

3. RESULTS AND DISCUSSION

Given that, in general, adsorbents and catalysts differ significantly in their thermal conductivity values, this factor, combined with the bed structure and the exothermic nature of adsorption, determines the efficiency of the sorption process. This is due to the significant influence of the structure of the hybrid bed on the axial and radial temperature profiles. In the present study, the average concentration of adsorbed carbon dioxide in the solid phase at the time of bed breakthrough was used as an index of the efficiency of the adsorption process. The breakthrough time, t_b, was defined as:

$$t_b = \min\{t : \overline{y}_{CO_2,out}(t) = c_{lim} \cdot y_{CO_2,in}\} \tag{31}$$

which states that t_b is the minimum time at which the average molar fraction of adsorbate at the reactor outlet, $\overline{y}_{CO_2,out}(t)$, reaches a predefined ratio, c_{lim} (here set to 1%), of the molar fraction of CO_2 in the gas feed to the apparatus, $y_{CO_2,in}$. Meanwhile, the average concentration at the breakthrough time, $Q_{CO_2}(t_b)$, was calculated from the equation:

$$Q_{CO_2}(t_b) = \frac{2\pi}{\pi R_r^2 L} \int_0^L \int_0^{R_r} f_{ads}\, q_{CO_2}|_{t_b}\, r\, dr dx \tag{32}$$

Comparative analysis of sorption dynamics was performed for three different bed configurations described in the previous section and shown in Fig. 2. For the bed made of a uniform physical mixture of adsorbent and catalyst particles (Fig. 2a) and for the layered bed (Fig. 2b), numerical simulations were conducted for both the adiabatic and nonadiabatic (with T_w = 298.15 K) cases. In these calculations, following the results of earlier work (Gunia et al., 2023), where the one-dimensional adiabatic case was analysed, the volume ratio of adsorbent to catalyst was also varied (i.e. *ads-to-cat* = $\{1:1, 2:1, 3:1, 4:1, 5:1, 6:1\}$). Moreover, for a layered bed the number

Table 1. The main parameters of the mathematical model.

Parameter	Value	Parameter	Value	Parameter	Value
a_0	$6.509 \cdot 10^{-3}$ mol/(kg·kPa)	L	1 m	$\varepsilon_{p,ads}$	0.54
b_0	$4.884 \cdot 10^{-4}$ 1/kPa	P	101325 Pa	$\varepsilon_{p,cat}$	0.6
c	$3.805 \cdot 10$ K	r_p	10^{-3} m	$\lambda_{s,ads}$	0.15 W/(m·K)
$c_{s,ads}$	1100 J/(kg·K)	$T_f = T_w$	298.15 K	$\lambda_{s,cat}$	0.84 W/(m·K)
$c_{s,cat}$	1107 J/(kg·K)	u	0.2 m/s	$\rho_{p,ads}$	1085 kg/m^3
d_{pore}	10^{-9} m	$y_{CO_2,in}$	0.05	$\rho_{p,cat}$	2355 kg/m^3
D_r	$5 \cdot 10^{-2}$ m	ΔH_{ads}	$-3.898 \cdot 10^4$ J/mol	τ_0	$7.487 \cdot 10^{-2}$
E	$2.991 \cdot 10^3$ K	ε_b	0.45	τ_p	3

of layers was changed as well ($M = \{2, 4, 6, 8, 10\}$). The calculations concerning the case of the bed with radially nonuniform sorbent distribution were limited to nonadiabatic case, and as specified above (Fig. 3a) two zones in such a bed were distinguished, i.e., a cylindrical core and a cylindrical shell, characterized by constant but different (among the zones) distributions of functionalities.

Figure 4 compares the results obtained for two values of the adsorbent to catalyst ratio versus the number of layers in the layered bed obtained for the adiabatic and nonadiabatic cases. The last (from the right) symbols corresponding to each analysed process case refer to a bed made of physical mixture of particles. As expected, the introduction of bed cooling (nonadiabatic case) enables a significant increase in bed breakthrough time (Fig. 4a) and raises the corresponding amount of adsorbed CO_2 (Fig. 4b). While the configuration with six alternating layers of adsorbent and catalyst performs best in the case of a process conducted without heat exchange, for the nonadiabatic case a mixed bed behaves slightly better.

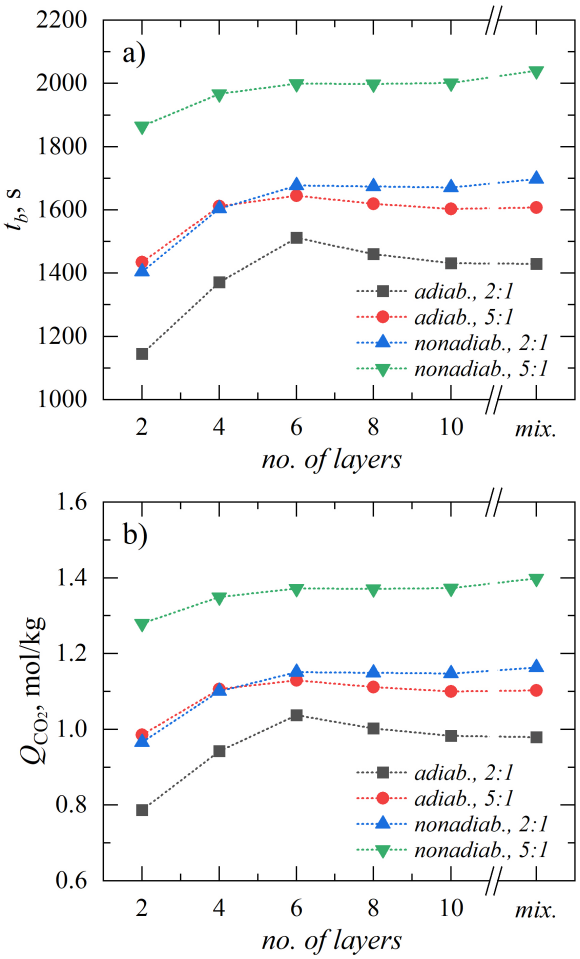

Figure 4. Bed breakthrough time, t_b (a), and corresponding values of the average adsorbate concentration in the sorbent, Q_{CO_2} (b), determined for adsorbent-to-catalyst ratios equal to 2:1 and 5:1, for both adiabatic and nonadiabatic ($T_w = 298.15$ K) bed vs. number of alternating layers.

Both in the adiabatic and nonadiabatic cases, the most significant increase in breakthrough time and the amount of adsorbed CO_2 is observed when moving from two to four zones. This is because the two-layer configuration behaves like a standard adsorption column, but with an additional sorption-inactive zone located near the outlet. In the case of catalyst (or inert) layers sandwiched between the sorbent layers (e.g. 4 to 10 layers), the initially cold sorption-inactive particles function as a heat sink for the gas being warmed up due to exothermic sorption. Thus, the t_b value is significantly lengthened and the Q_{CO_2} value is increased even in the absence of bed cooling (Fig. 4). The improvement of the bed behaviour under adiabatic conditions, achieved by structuring the bed with alternating layers of adsorbent and inert material, was described in a previous work where the characteristic formation of heat waves was analyzed, allowing the inert layer to be considered as a heat sink (Gunia et al., 2023). In addition, the same work by Gunia et al. (2023) showed that the optimal number of layers under adiabatic conditions is six. However, Figs. 4a and 4b show that when the cooling effect of a wall maintained at a lower temperature is added, the adoption of a uniform mixture configuration improves the bed performance and the optimal number of layers is no longer equal to six. This is because the phenomenon that affects the bed sorption efficiency is not only the presence of a thermal flywheel, but also the enhanced ability of the bed to transport heat out of the reactor. This effect is consistent with the experimental results shown in the work of Demir et al. (2010) and Ben-Mansour et al. (2020). Specifically, in the work of Demir et al. (2010), it was experimentally shown that mixing metal pieces uniformly with the adsorbent improves the conductivity of the bed and thus the removal of heat generated during adsorption. Unlike Demir et al. (2010), the present work aims to understand not only the variability of the adsorption efficiency while varying the ratio of the amount of adsorbent to inert material, but also to push the analysis towards the bed structure, which can be of fundamental importance in adsorption processes, as shown in the experimental work of Jarczewski et al. (2022).

The heat sink effect is still dominant in the layered nonadiabatic configuration and is shown in more detail in Fig. 5, for the number of layers $M = 6$ and the nonadiabatic case with adsorbent to catalyst ratio equal to 5:1. The left column of Fig. 5 illustrates the spatial distributions of temperature, $T(x, r)$, at several representative time instants, while the right column shows the concentration of CO_2 adsorbed in the solid per unit volume of the reactor, determined according to the formula:

$$\tilde{q}_{CO_2} = \rho_{b,\mathrm{ads}} f_{\mathrm{ads}} q_{CO_2} \tag{33}$$

As shown in Fig. 5a, the adsorption process is accompanied by the formation of a classical thermal wave. However, once the wave front reaches the boundary of the first zone of the sorbent and catalyst (vertical dashed line), due to the absence of adsorption occurring in the catalyst (Fig. 5b), a drop in temperature is observed, which is due to the large

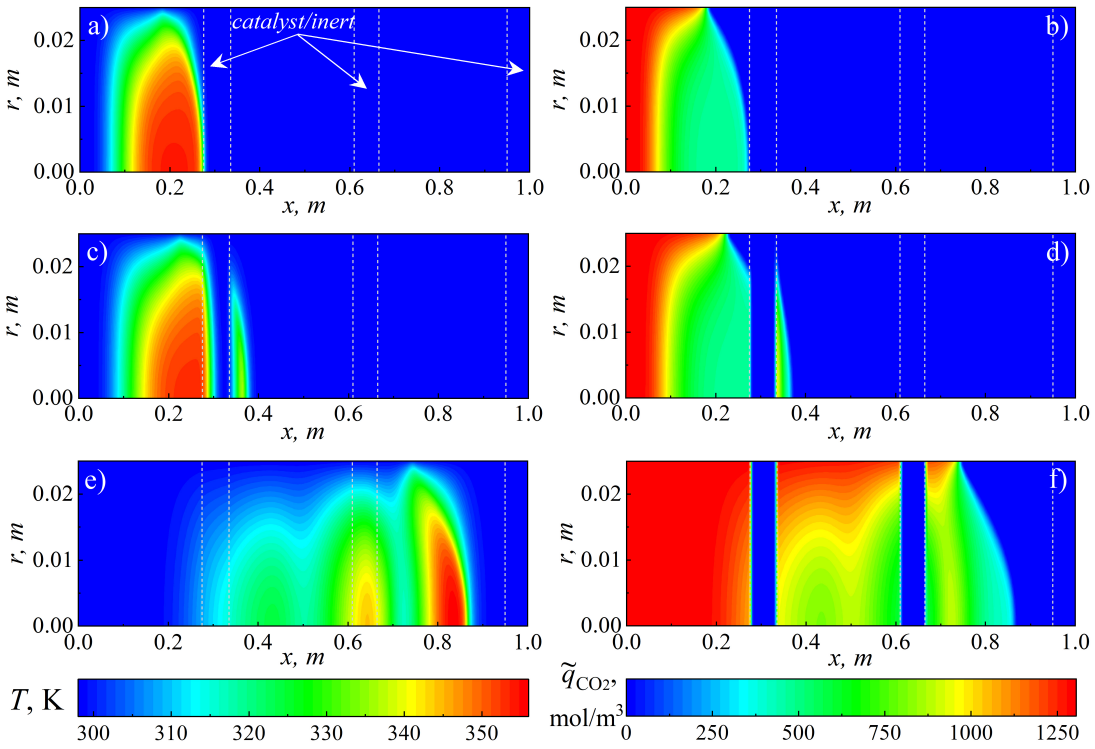

Figure 5. Spatial distributions of temperature (left column) and solid-phase concentration of CO_2 (right column) expressed in moles per cubic meter of hybrid reactor determined for nonadiabatic ($T_w = 298.15$ K) hybrid bed with six alternating layers of adsorbent and catalyst, and with adsorbent-to-catalyst ratio equal to 5:1 at: (a)–(b) $t = 8$ min, (c)–(d) $t = 10$ min, and (e)–(f) $t = 30$ min.

heat capacity of the bed material within this zone. As a result, the influent gas on the subsequent second sorbent zone is slightly cooler (Fig. 5c) and the adsorption equilibrium is more favourable (Fig. 5d). Moving forward in time, the effect of heat uptake by the catalyst (inert) layer diminishes due to its heating and the flattening of the thermal waves resulting from axial heat conduction throughout the bed (Fig. 5e).

Figure 6 shows a comparison of the spatial distributions of the temperature and the variable $\tilde{q}_{CO_2}$ at t_b obtained for different bed configurations, i.e.: layered bed with $M = 2$ (Figs. 6a and 6b), bed made of uniform mixture of particles (Figs. 6c and 6d), and layered bed with $M = 6$ (Figs. 6e and 6f). As mentioned earlier, a uniform nonadiabatic bed slightly outperforms a multilayer bed regarding breakthrough time, that is $t_b = 1999.36$ s for the latter and $t_b = 2039.97$ s for uniformly mixed sorbent and catalyst particles. Furthermore, analysing Figures 6a, 6c and 6e, it is evident that higher temperatures are observed near the outlet section when dealing with a layered configuration, compared to the uniform mixture configuration. This may be related to the fact that the preferred path for heat exchange is where the catalyst is present. In the case of the layered configuration, the catalyst is not present where adsorption occurs, making it difficult for heat to be removed from the bed due to the higher resistance compared to the uniform case, especially near the wall. In fact, heat removal through the wall of the apparatus in the sorption zones, where the actual process takes place, is hindered due to the lower heat conductivity value of zeolite 13X compared to the nickel catalyst (respectively, $\lambda_{s,ads} = 0.15$ W/(m·K) and $\lambda_{s,cat} = 0.84$ W/(m·K)). Consequently, the physical mixture of adsorbent and catalyst exhibits an improvement of the apparent wall heat transfer coefficient (h_w) and of the effective radial thermal conductivity (K_{rad}) (see Eq. (14) and (28)), thereby facilitating heat extraction. Hence, with the aim of enhancing the cooling effect, a configuration with a radially nonuniform distribution of the sorbent volume fraction is considered in the next step.

The analysis of the temperature distributions shown in Figs. 6a, 6c and 6e suggests that for the bed configuration composed of a cylindrical core with $f_{ads,1}$ and $f_{cat,1}$ and of cylindrical shell characterized by $f_{ads,2} \neq f_{ads,1}$ and $f_{cat,2} \neq f_{cat,1}$ (Fig. 3a), placing more sorbent near the wall (i.e. $f_{ads,2} > f_{ads,1}$) could be more advantageous due to the lower temperature near the wall, which favours adsorption. This approach, however, is also disadvantageous, because the adsorbent near the wall has lower thermal conductivity, which negatively impacts the efficiency of heat transfer, thereby worsening the apparent wall heat transfer coefficient. The key factor increasing sorption efficiency is the intensified heat removal through the wall.

Even with the assumption made here about the constant character of $f_{ads,1}$ and $f_{ads,2}$ in the cylindrical core and surrounding shell, respectively, the number of viable solutions is

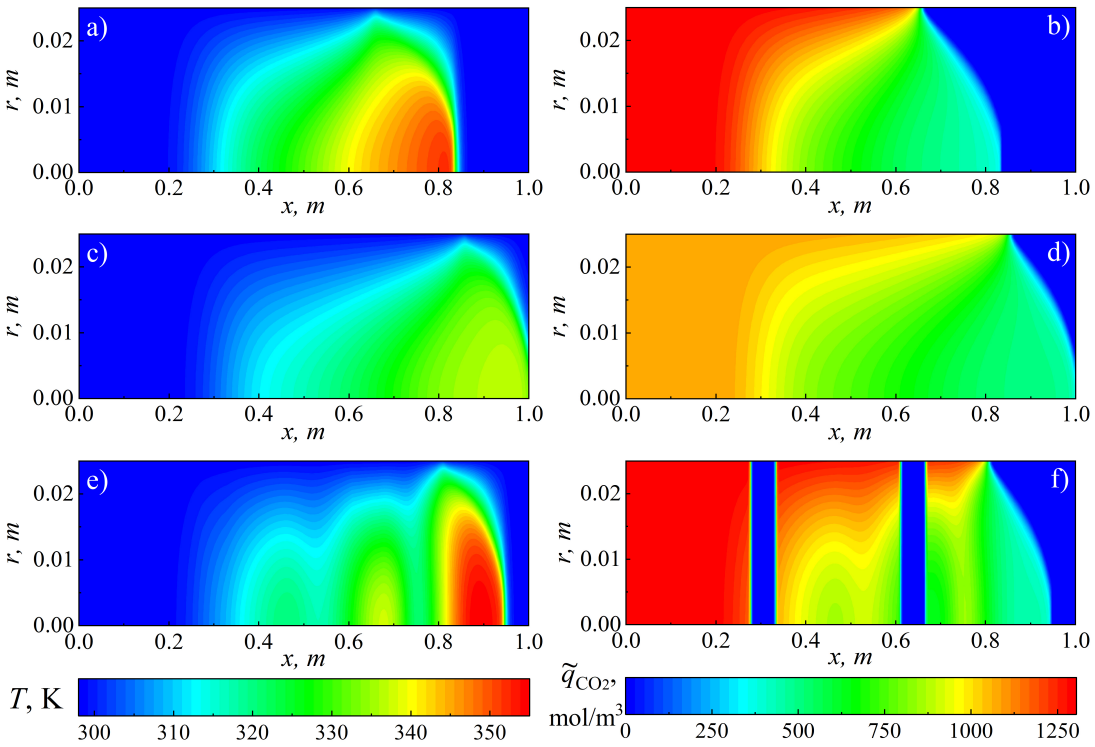

Figure 6. Spatial distributions of temperature (left column) and solid-phase concentration of CO_2 (right column) expressed in moles per cubic meter of hybrid reactor at t_b for: (a)–(b) bed with two layers ($t_b = 1864.93$ s), (c)–(d) bed made of uniform mixture of particles ($t_b = 2039.97$ s), and (e)–(f) bed with six layers ($t_b = 1999.36$ s). In all cases, the bed is nonadiabatic ($T_w = 298.15$ K), and adsorbent-to-catalyst ratio is 5:1.

essentially infinite, because an additional design parameter is the radius of the core. For this reason, to determine the radial distribution of the sorbent, which could give a higher sorption efficiency than the uniform and layered bed, an optimization problem was solved. The average value of CO_2 adsorbed in the bed up to the breakthrough time, Q_{CO_2}, was chosen as the objective function, therefore as a result, the problem became:

$$\max_{f_{ads,1},R_c} Q_{CO_2} \tag{34}$$

In the above equation, $f_{ads,1}$ is the volume fraction of sorbent in the core, and R_c is the radius of the core. Given that for a fixed value of the ratio of sorbent to catalyst (here 5:1), $f_{ads,2}$ depends on $f_{ads,1}$, the constraints of the problem can be written as follows:

$$f_{ads,2} = \frac{f_{ads,tot} - f_{ads,1}\,(V_1/V_{tot})}{(V_2/V_{tot})} \tag{35}$$

where $f_{ads,tot} = \text{ads-to-cat}/\,(\text{ads-to-cat} - 1)$ is the total volumetric fraction allocated to the adsorbent in the reactor, V_1 and V_2 are respectively the volumes of the inner bed core and the outer bed shell, whereas V_{tot} is the total volume of the reactor. Moreover, both $f_{ads,1}$ and $f_{ads,2}$ must be constrained to be equal to or greater than 0 and less than or equal to 1. These inequalities combined with Eq. (35), divide the region of the space spanned by all the combinations of $f_{ads,1}$ and R_c into a feasible and an unfeasible region, which is displayed in Fig. 7.

Since the solution of the optimization problem at this research stage is mainly illustrative, the problem was solved using a brute force approach. Some experimental work to validate the model results is currently being designed for future work based on the results of this numerical analysis. Figure 7 shows feasible solutions of the problem defined by Eqs. (34) and (35) in the space of design parameters determined by direct simulation of the dynamics of the hybrid bed model until its breakthrough. In addition, the optimal pair of design parameters, namely $f_{ads,1} = 1$ and $R_c/R_r = 0.5$ (hence $R_c = 1.25 \cdot 10^{-2}$ m), for which $Q_{CO_2} = 1.431$ mol/kg, are marked in the figure with a bullet. For such a solution, given the adopted value of the adsorbent to catalyst ratio (5:1) throughout the apparatus, $f_{ads,2} = 0.78$. The optimum point can be seen as a compromise between improving the wall heat transfer and the radial heat conductivity. In fact, since both effects are influenced by the conductivity of the bed material (see Eqs. (14) and (28)), for a constant adsorbent to catalyst volume ratio, improving one effect inevitably worsens the other. As a result, if the catalyst is positioned entirely near the wall, the heat generated in the bed will have difficulty reaching the higher conductivity layer, making it more difficult to extract and reducing the performance of the adsorbent bed. In Fig. 8, the resulting configuration (denoted by *rad. nonadiab.*) is compared with the results obtained for the layered bed (denoted by *lay. adiab.* and *lay. nonadiab.*) and the uniform bed (denoted by *mix. adiab.* and *mix. nonadiab.*). The results are

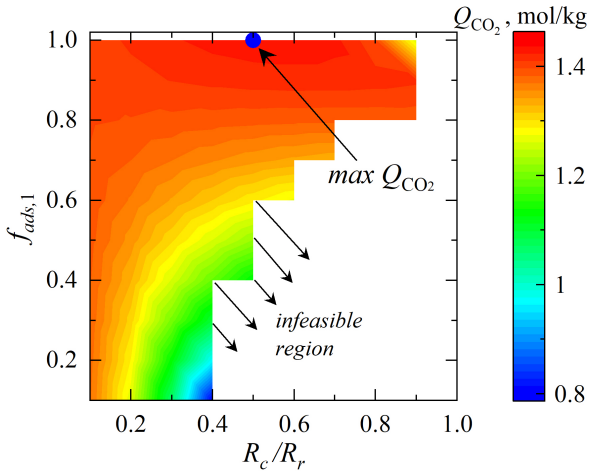

Figure 7. Objective function, Q_{CO_2}, for optimizing the structure of nonadiabatic bed with the radially nonuniform distribution of adsorbent, comprising two decision variables, i.e., core radius, R_c, and volume fraction of sorbent particles in the core, $f_{ads,1}$, together with its maximum (denoted with bullet). Optimization was done by setting $T_w = 298.15$ K and the adsorbent-to-catalyst ratio equal to 5:1.

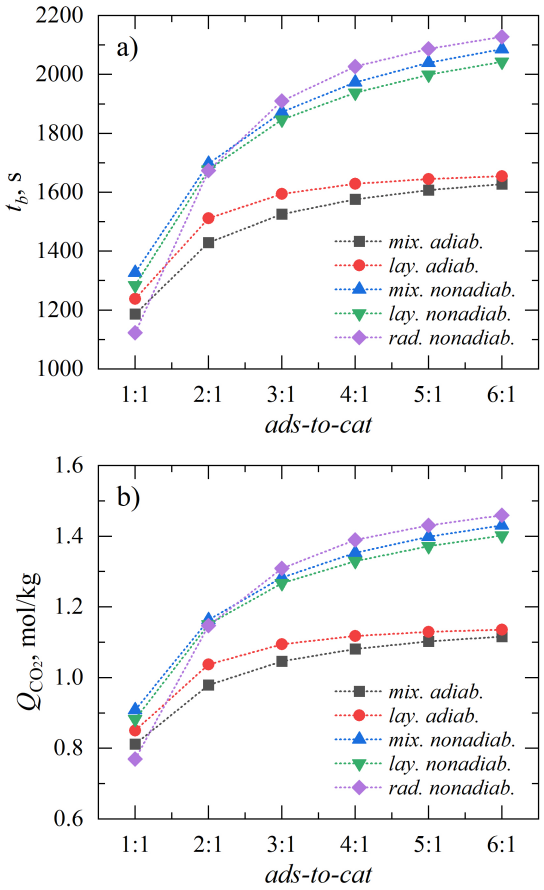

Figure 8. Bed breakthrough time, t_b (a), and corresponding values of the average adsorbate concentration in the sorbent, Q_{CO_2} (b), determined for different configurations of hybrid bed depending on adsorbent-to-catalyst ratio, where *mix.* denotes a bed made of uniform mixture of particles, *lay.* corresponds to a bed made of six alternating layers, and *rad.* denotes bed with optimal radially nonuniform distribution of adsorbent.

shown as a function of the sorbent to catalyst ratio. It can be observed that in the case of the aforementioned ratio equal to 5:1 (which was addressed by the solved optimization problem) the radial nonuniform distribution of the sorbent allows to increase both the t_b and Q_{CO_2} when compared to the mixed or layered configuration. Although the increase is not large, it indicates a potentially important direction for structuring hybrid beds in adsorptive reactors. Figures 9 and 10 show, respectively, the spatial distributions of temperature and CO_2 concentration in the solid phase (expressed per unit of volume in the column) at breakthrough (Fig. 9) and shortly after the start of the process, i.e. for $t = 10$ min (Fig. 10). The figures show both the distributions for the optimal solution (Figs. 9a and 9b, and Figs. 10a and 10b) and for the case with the same value of R_c where most of the sorbent is located near the wall (Figs. 9c and 9d, and Figs. 10c and 10d, where $f_{ads,1} = 0.4$ and $f_{ads,2} = 0.98$). It can be observed that both at the beginning of the process (Fig. 10) and at the breakthrough of the bed (Fig. 9), both the front of the concentration wave and the thermal wave for the optimal solution are much more flattened than those obtained for the second case shown here. There are two reasons for this: For the optimal solution, heat removal from the core is difficult but in this zone there is more sorbent available for the CO_2. As a result, the axial mass dispersion flattens the longitudinal concentration wave to a lesser extent because the adsorbate is effectively adsorbed by the solid. At the same time, the more effective heat removal from the cylindrical shell (characterized by higher nickel content) reduces the width of the thermal wave near the apparatus wall, which can be observed most clearly in Figure 10. For the optimal solution (Figs. 10a and 10b), the heat removal from the core is difficult, but in this zone there is more sorbent available for CO_2. As a result, the axial mass dispersion flattens the concentration wave in the longitudinal direction to a lesser extent, as can be seen by comparing Figures 10b and 10d, since the adsorbate is effectively adsorbed by the solid. In addition, the bed zone characterized by a lower fraction of adsorbent performs better in the optimal case (Fig. 10b), showing higher CO_2 concentration in the solid phase than in the sub-optimal case (Fig. 10d). At the same time, more effective heat removal from the cylindrical shell (characterized by higher nickel content) reduces the width of thermal wave near the apparatus wall (Fig. 10a). Furthermore, Figs. 9 and 10 show that by radially distributing materials with different capacities and thermal conductivities, it is possible to significantly modify both the shape and the intensity of the heat wave generated inside the bed, in this case due to adsorption. This new ability to manage heat can be exploited even more during the subsequent reactive phase. In the latter, the heat release must be carefully balanced in order to avoid the formation of hot spots, thus preventing too rapid desorption and achieving the minimum temperature required for catalytic reaction to take place.

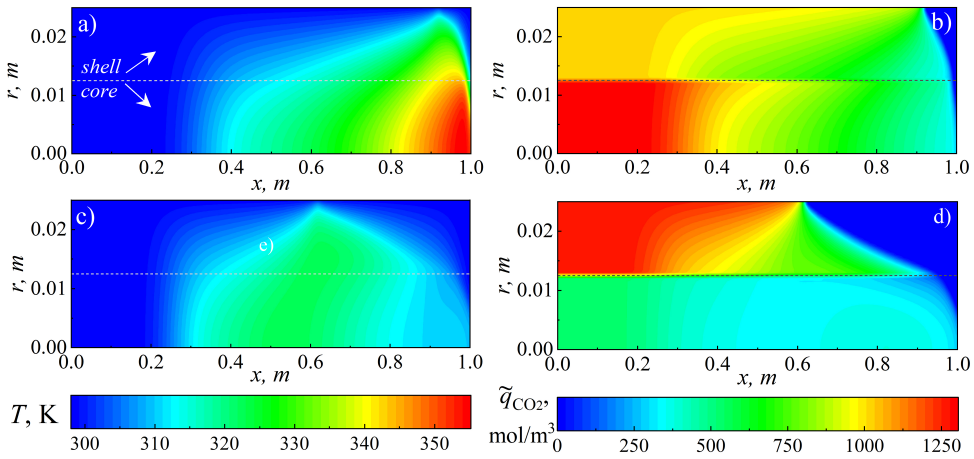

Figure 9. Spatial distributions of temperature (left column) and solid-phase concentration of CO_2 (right column) expressed in moles per cubic meter of hybrid reactor at t_b for bed with radially nonuniform distribution of adsorbent: (a)–(b) optimal design with $f_{ads,1} = 1$ and $R_c/R_r = 0.5$ ($t_b = 2087.29$ s), and (c)–(d) configuration with $f_{ads,1} = 0.4$ and $R_c/R_r = 0.5$ ($t_b = 1639.39$ s). In both cases, the bed is nonadiabatic ($T_w = 298.15$ K), and the adsorbent-to-catalyst ratio is 5:1.

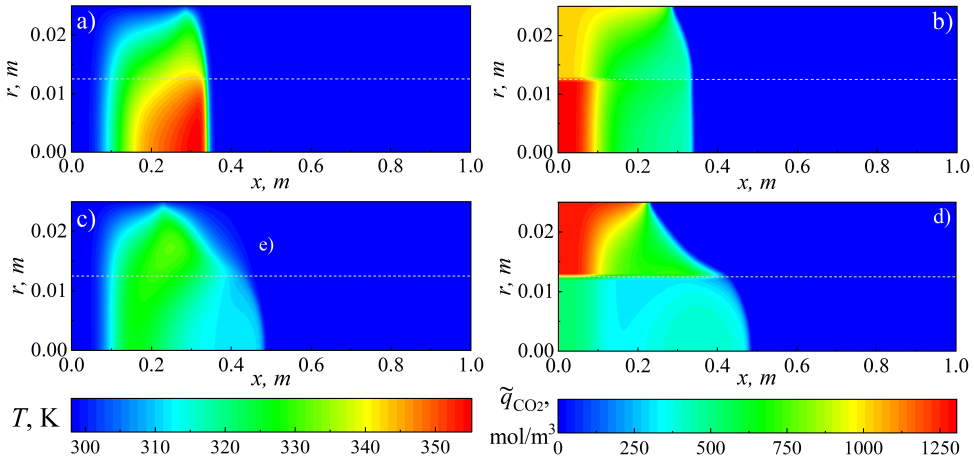

Figure 10. Spatial distributions of temperature (left column) and solid-phase concentration of CO_2 (right column) expressed in moles per cubic meter of hybrid reactor determined for nonadiabatic ($T_w = 298.15$ K) hybrid bed with radially nonuniform distribution of adsorbent, and with adsorbent-to-catalyst ratio equal to 5:1 at $t = 10$ min: (a)–(b) optimal design with $f_{ads,1} = 1$ and $R_c/R_r = 0.5$, and (c)–(d) configuration with $f_{ads,1} = 0.4$ and $R_c/R_r = 0.5$.

4. CONCLUSIONS

In this study, the dynamics of a nonadiabatic and adiabatic hybrid bed was analysed using a two-dimensional mathematical model to account for both longitudinal and radial distributions of concentration and temperature. The effect of different sorbent and catalyst spatial arrangements in the hybrid bed on its performance during CO_2 adsorption step was investigated.

It was shown that in both the adiabatic and nonadiabatic cases a bed with alternating layers of adsorbent and catalyst and a bed in the form of a physical mixture of the two types of particles outperforms a standard adsorption bed in terms of bed breakthrough time and sorption capacity. Although the latter was not explicitly studied in the paper, the structure analysed, with two axial layers, is equivalent to a classical adsorption column, but with a sorption inert zone located near the outlet. The improvement in the performance was attributed to the influence of the catalyst on the heat transport inside the bed; in fact, the catalyst, as opposed to the adsorbent, was characterized by both a higher thermal conductivity and a higher heat capacity, thus acting locally as a heat sink.

The optimization problem was solved for a configuration with radially nonuniform adsorbent distribution, and it was further shown that placing more catalysts (characterized by higher thermal conductivity) close to the wall allowed to extend the bed breakthrough time and the sorption capacity. This is due to the much more efficient removal from the bed of the heat generated in the exothermic adsorption process.

Since the hybrid apparatus analysed in this paper is intended to be used in the second step of the cyclic process of CO_2 methanation, additional questions arise that will be the subject of further research. Indeed, it is clear that the optimization of the hybrid bed must be carried out for the entire two-step process, i.e. adsorption and reactive regeneration.

This is a multi-criteria problem, where the objective functions could be the sorption capacity of the bed (for the adsorption step) and the degree of conversion of CO_2 in the reaction with the hydrogen fed to the bed (for the regeneration step). Regarding the latter, given exothermic nature of the methanation process, it is expected to be advantageous to place more catalyst close to the walls of the apparatus. However, a core containing only sorbent (which is the mass source at the adsorption stage) may not be the best solution due to limited radial mass transport.

Acknowledgements

The research was financed by the Polish National Science Centre under the research project "Experimental and numerical analysis of mass and heat transport in "tailor-made" fixed beds for gas-solid processes", no. UMO-2021/42/E/ST8/00313.

SYMBOLS

a, a_0	parameters in the Toth isotherm equation (Eqs. (7) and (8)), mol/(kg·kPa)
a_{ax}, a_{rad}	parameters of the convective term in the expression for determination, respectively, of axial and radial thermal conductivity (Eqs. (12) and (13))
A	slope of the function defined by Eq. (29) and Eq. (30)
b, b_0	parameters in the Toth isotherm equation (Eqs. (7) and (8)), 1/kPa
c	parameter in the Toth isotherm equation (Eqs. (7) and (8)), K
c_g	gas specific heat capacity, J/(kg·K)
$c_{g,\mathrm{ads}}$	adsorbed phase specific heat capacity, J/(kg·K)
c_{lim}	ratio of molar fractions in Eq. (31)
c_s	solid specific gas capacity, J/(kg·K)
C_{CO_2}	molar concentration of CO_2 in gas phase, mol/m^3
C_{f,CO_2}	molar concentration of CO_2 in gas phase at the inlet, mol/m^3
d_p	particle diameter, m
d_{pore}	mean pore diameter, m
D_{ax}	axial mass dispersion coefficient, m^2/s
D_e	effective diffusion coefficient, m^2/s
D_K	Knudsen diffusion coefficient, m^2/s
D_m	molecular diffusion coefficient, m^2/s
D_r	reactor diameter, m
D_{rad}	radial mass dispersion coefficient, m^2/s
E	parameter in the Toth isotherm equation (Eqs. (7) and (8)), K
f_{ads}	volume fraction of adsorbent in the bed, –
f_{cat}	volume fraction of catalyst in the bed, –
h_w	apparent wall heat transfer coefficient, W/(m^2·K)
k	mass transfer coefficient in LDF model given by Eqs. (5) and (6), 1/s
K_{ax}	axial effective thermal conductivity, W/(m·K)
K_{rad}	radial effective thermal conductivity, W/(m·K)
K_{ax}^0	axial static effective thermal conductivity, W/(m·K)
K_{rad}^0	radial static effective thermal conductivity, W/(m·K)
L	reactor length, m
M	number of sorbent and catalyst layers in the layered bed, –
N_{ax}	number of discretization nodes along the bed length, –
N_{rad}	number of discretization nodes along the bed radius, –
Nu	Nusselt number, –
p	total pressure,
p_{CO_2}	CO_2 partial pressure,
Pr	Prandtl number, –
r	radial coordinate, m
r_p	particle radius, m
R	universal gas constant, J/(mol·K)
R_c	radius of the cylindrical core, m
R_r	reactor radius, m
Re_p	particle Reynolds number, –
q_{CO_2}	concentration of CO_2 adsorbed in the solid phase, mol/kg
$q^*_{CO_2}$	equilibrium concentration of CO_2 adsorbed in the solid phase, mol/kg
$\tilde{q}_{CO_2}$	concentration of CO_2 adsorbed in the solid phase expressed per unit volume of the column defined by Eq. (33), mol/m^3
Q_{CO_2}	average concentration of adsorbed CO_2 at t_b defined by Eq. (32), mol/kg
Sc	Schmidt number, –
t	time, s
t_b	time of breakthrough of the bed, s
T	temperature, K
T_0	initial bed temperature, K
T_f	gas temperature at the inlet, K
T_w	wall temperature, K
u	superficial gas velocity, m/s
V	volume, m^3
$y_{CO_2,\mathrm{in}}$	molar fraction of CO_2 in the gas stream at the inlet, –
$\overline{y}_{CO_2,\mathrm{out}}$	average molar fraction of CO_2 in the gas stream at the outlet, –
x	axial coordinate, m

Greek symbols

β	parameter in the correlation for static effective thermal conductivity (Eq. (14))
γ	parameter in the correlation for static effective thermal conductivity (Eq. (14))
Γ_{heat}	parameter in the mass balance equation (1) defined by Eq. (3)
Γ_{mass}	parameter in the mass balance equation (2) defined by Eq. (4)
ΔH_{ads}	isosteric enthalpy of CO_2 adsorption, J/mol
ε_b	bed porosity, –
ε_p	particle porosity, –

ε_t	total porosity of the bed, –
κ	the ratio of the thermal conductivity of a solid to a gas, –
λ_g	thermal conductivity of the gas, W/(m·K)
λ_s	thermal conductivity of the solid, W/(m·K)
μ_g	gas viscosity, kg/m^3
ρ_g	gas density, kg/m^3
ρ_b	bed bulk density, kg/m^3
τ, τ_0	parameters in the Toth isotherm equation (Eqs. (7) and (8)), –
τ_p	tortuosity factor, –
ψ_t	parameter in the correlation for static effective thermal conductivity (Eq. (14))

Subscripts

1	refers to the inner part (core) of the fixed bed
2	refers to the outer part (shell) of the fixed bed
ads	refers to adsorbent or adsorbate
cat	refers to catalyst
tot	refers to total

REFERENCES

Abd A.A., Othman M.R., Helwani Z., Kim J., 2024. An overview of biogas upgrading via pressure swing adsorption: navigating through bibliometric insights towards a conceptual framework and future research pathways. *Energy Convers. Manage.*, 306, 118268. DOI: 10.1016/j.enconman.2024.118268.

Ben-Mansour R., Abuelyamen A., Qasem N.A.A., 2020. Thermal design and management towards high capacity CO_2 adsorption systems. *Energy Convers. Manage.*, 212, 112796. DOI: 10.1016/j.enconman.2020.112796.

Bremer J., Rätze K.H.G., Sundmacher K., 2017. CO_2 methanation: Optimal start-up control of a fixed-bed reactor for power-to-gas applications. *AIChE J.*, 63, 23–31. DOI: 10.1002/aic.15496.

Chauhan P.R., Kaushik S.C., Tyagi S.K., 2022. A review on thermal performance enhancement of green cooling system using different adsorbent/refrigerant pairs. *Energy Convers. Manage.: X,* 14, 100225. DOI: 10.1016/j.ecmx.2022.100225.

Demir H., Mobedi M., Ülkü S., 2010. The use of metal piece additives to enhance heat transfer rate through an unconsolidated adsorbent bed. *Int. J. Refrig.*, 33, 714–720. DOI: 10.1016/j.ijrefrig.2009.12.032.

Díaz-Heras M., Belmonte J.F., Almendros-Ibáñez J.A., 2020. Effective thermal conductivities in packed beds: Review of correlations and its influence on system performance. *Appl. Therm. Eng.*, 171, 115048. DOI: 10.1016/j.applthermaleng.2020.115048.

Dixon A.G., 2012. Fixed bed catalytic reactor modelling – the radial heat transfer problem. *Can. J. Chem. Eng.*, 90, 507–527. DOI: 10.1002/cjce.21630.

Dixon A.G., Paterson W.R., Cresswell D.L., 1978. Heat transfer in packed beds of low tube/particle diameter ratio. In: Weekman Jr. V.W., Luss D. (Eds.), *Chemical reaction Engineering – Houston. ACS Symposium Series*, 65, 238–253. DOI: 10.1021/bk-1978-0065.ch020.

Do D.D., 1998. *Adsorption analysis: Equilibria and kinetics*. Imperial College Press, London. DOI: 10.1142/p111.

Eppinger T., Jurtz N., Kraume M., 2021. Influence of macroscopic wall structures on the fluid flow and heat transfer in fixed bed reactors with small tube to particle diameter ratio. *Processes*, 9, 689. DOI: 10.3390/pr9040689.

Glueckauf E., Coates J.I., 1947. 241. Theory of chromatography. Part IV. The influence of incomplete equilibrium on the front boundary of chromatograms and on the effectiveness of separation. *J. Chem. Soc.*, 1315–1321. DOI: 10.1039/JR9470001315.

Grande C. A., Kaiser A., Andreassen K.A., 2023. Methane storage in metal-organic framework HKUST-1 with enhanced heat management using 3D printed metal lattices. *Chem. Eng. Res. Des.*, 192, 362–370. DOI: 10.1016/j.cherd.2023.03.003.

Gunia M., Ciećko J., Bizon K., 2023. Assessment of bed macrostructuring and thermal wave impact on carbon dioxide adsorption efficiency in a hybrid fixed-bed reactor. *Chem. Process Eng.*, 44, e13. DOI: 10.24425/cpe.2023.144699.

Jarczewski S., Barańska K., Drozdek M., Michalik M., Bizon K., Kuśtrowski P., 2022. Energy-balanced and effective adsorption-catalytic multilayer bed system for removal of volatile organic compounds. *Chem. Eng. J.*, 431, 133388. DOI: 10.1016/j.cej.2021.133388.

Jorge L.M.M., Jorge R.M.M., Giudici R., 2010. Experimental and numerical investigation of dynamic heat transfer parameters in packed bed. *Heat Mass Transfer*, 46, 1355–1365. DOI: 10.1007/s00231-010-0659-6.

Kammerer S., Borho I., Jung J., Schmidt M.S., 2023. Review: CO_2 capturing methods of the last two decades. *Int. J. Environ. Sci. Technol.*, 20, 8087–8104. DOI: 10.1007/s13762-022-04680-0.

Kunii D., Smith J.M., 1960. Heat transfer characteristics of porous rocks. *AIChE J.*, 6, 71–78. DOI: 10.1002/aic.690060115.

Kwan T.H., Yao Q., 2022. Numerical analysis on the geometrical design of liquid cooling based carbon capture by adsorption for higher thermal efficiency. *Int. Commun. Heat Mass Transfer,* 139, 106459. DOI: 10.1016/j.icheatmasstransfer.2022.106459.

Leonzio G., Shah N., 2024. Recent advancements and challenges in carbon capture, utilization and storage. *Curr. Opin. Green Sust*ainable Chem., 46, 100895. DOI: 10.1016/j.cogsc.2024.100895.

Lian Y., Deng S., Li S., Guo Z., Zhao L., Yuan X., 2019. Numerical analysis on CO_2 capture process of temperature swing adsorption (TSA): optimization of reactor geometry. *Int. J. Greenhouse Gas Control*, 85, 187–198. DOI: 10.1016/j.ijggc.2019.03.029.

Lin X., Li X., Liu H., Boczkaj G., Cao Y., Wang C., 2024. A review on carbon storage via mineral carbonation: bibliometric analysis, research advances, challenges, and perspectives. *Sep. Purif. Technol.,* 338, 126558. DOI: 10.1016/j.seppur.2024.126558.

Martins V.F.D., Miguel C.V., Gonçalves J.C., Rodrigues A.E., Madeira L.M., 2022. Modeling of a cyclic sorption–desorption unit for continuous high temperature CO_2 capture from flue gas. *Chem. Eng. J.*, 434, 134704. DOI: 10.1016/j.cej.2022.134704.

McLaughlin H., Littlefield A.A., Menefee M., Kinzer A., Hull T., Sovacool B.K., Bazalian M.D., Kim J., Griffiths S., 2023. Carbon capture utilization and storage in review: sociotechnical implications for a carbon reliant world. *Renew. Sustain. Energy Rev.*, 177, 113215. DOI: 10.1016/j.rser.2023.113215.

Miguel C.V., Soria M.A., Mendes A., Madeira L.M., 2017. A sorptive reactor for CO_2 capture and conversion to renewable methane. *Chem. Eng. J.*, 332, 590–602. DOI: 10.1016/j.cej.2017.04.024.

Poling B.E., Prausnitz J.M., O'Connell J.P., 2001. *Properties of gases and liquids*. 5th edition, McGraw-Hill Education, New York.

Saha B.B., Uddin K., Pal A., Thu K., 2019. Emerging sorption pairs for heat pump applications: an overview. *JMST Adv.*, 1, 161–180. DOI: 10.1007/s42791-019-0010-4.

Stegehake C., Riese J., Grünewald M., 2018. Aktueller Stand zur Modellierung von Festbettreaktoren und Möglichkeiten zur experimentellen Validierung. *Chem. Ing. Tech.*, 90, 1739–1758. DOI: 10.1002/cite.201800130.

Szyc M., Nowak W., 2014. Operation of an adsorption chiller in different cycle time conditions. *Chem. Process Eng.*, 35, 109–119. DOI: 10.2478/cpe-2014-0008.

Tsotsas E., Schlünder E.-U., 1990. Heat transfer in packed beds with fluid flow: remarks on the meaning and the calculation of a heat transfer coefficient at the wall. *Chem. Eng. Sci.*, 45, 819–837. DOI: 10.1016/0009-2509(90)85005-X.

van Antwerpen W., du Toit C.G., Rousseau P.G., 2010. A review of correlations to model the packing structure and effective thermal conductivity in packed beds of mono-sized spherical particles. *Nucl. Eng. Des.*, 240, 1803–1818. DOI: 10.1016/j.nucengdes.2010.03.009.

Wakao N., Funazkri T., 1978. Effect of fluid dispersion coefficients on particle-to-fluid mass transfer coefficients in packed beds: correlation of sherwood numbers. *Chem. Eng. Sci.*, 33, 1375–1384. DOI: 10.1016/0009-2509(78)85120-3.

Wang Y., LeVan M.D., 2009. Adsorption equilibrium of carbon dioxide and water vapor on zeolites 5A and 13X and silica gel: pure components. *J. Chem. Eng. Data*, 54, 2839–2844. DOI: 10.1021/je800900a.

Weinstein M.J., Rao A.V., 2017. Algorithm 984: ADiGator, a toolbox for the algorithmic differentiation of mathematical functions in MATLAB using source transformation via operator overloading. *ACM Trans. Math. Softw.*, 44, 21. DOI: 10.1145/3104990.

Yagi S., Kunii D., 1960. Studies on heat transfer near wall surface in packed beds. *AIChE J.*, 6, 97–104. DOI: 10.1002/aic.690060119.

Yagi S., Kunii D., Wakao N., 1960. Studies on axial effective thermal conductivities in packed beds. *AIChE J.*, 6, 543–546. DOI: 10.1002/aic.690060407.